JOURNAL OF SOLID STATE CHEMISTRY 107, 554–562 (1993)

Studies on the Linear Chain Antiferromagnets: Ba_2MnX_3 (X = S, Se, Te) and Their Solid Solutions

M. A. GREANEY

Corporate Research, Exxon Research and Engineering Company, Annandale, New Jersey 08801

AND K. V. RAMANUJACHARY, Z. TEWELDEMEDHIN AND M. GREENBLATT

Department of Chemistry, Rutgers, The State University of New Jersey, New Brunswick, New Jersey 08903

Received November 16, 1992; in revised form April 23, 1993; accepted April 28, 1993

The linear chain antiferromagnetism previously reported for Ba_2MnS_3 and Ba_2MnSe_3 is now demonstrated for Ba_2MnTe_3. The mixed-chalcogenide solid solutions $Ba_2MnX_xX'_{3-x}$ (X, X' = S, Se, Te; x = 0, 1, 2) have been prepared and their electrical and magnetic properties studied. All of the phases are insulating with room temperature resistivities of approximately 10^2–10^3 Ω cm. The magnetic susceptibility curves of these mixed-chalcogenide phases exhibit broad maxima typical of one dimensional magnetic ordering. The linear-chain model of Bonner–Fisher for Heisenberg-type ions was applied to the susceptibility data. The geometry of the superexchange pathway appears to be critical in determining the strength of the magnetic coupling, with the polarizability of the bridging atom having little effect. © 1993 Academic Press, Inc.

Introduction

The synthesis of Ba_2MnS_3 and Ba_2MnSe_3 was first reported by Grey and Steinfink, in 1971 (*1*). These authors reported magnetic susceptibility measurements on the two phases and found that the observed data could be fit well by the classical spin model of Bonner and Fisher (*2*). This allows one to fit the observed magnetic susceptibility behavior with a theoretical equation providing an estimate of the Mn–Mn magnetic coupling. In 1977, the synthesis and single-crystal structure of the tellurium analogue Ba_2MnTe_3, was reported, and it was found to be isostructural with the sulfide and selenide analogues (*3*). The magnetic and electrical transport properties of the latter phase were not reported.

The Ba_2MnX_3 (X = S, Se, Te) phases are isostructural and crystallize in the orthorhombic space group *Pnma*. The Mn^{2+} ions are in a distorted tetrahedral coordination covalently bonded to four chalcogenide anions. These MnX_4 tetrahedra form infinite linear chains ($[MnX_2X_{2/2}]_n^{4n-}$) through corner-sharing with the chain axis parallel to the b axis. This is illustrated in Fig. 1. Here the view is perpendicular to the chain axis. The Mn–Mn separation along the chain is 4.31, 4.47, and 4.73 Å for the sulfide, selenide, and telluride respectively (*1*, *3*). The MnX_4^{4-} tetrahedra are distorted, with the X–Mn–X angles along the chain being 119.8, 118.5, and 116.3 for the sulfide, selenide, and telluride respectively. The two crystallographically independent Ba^{2+} ions are in seven-fold coordination between the chains with six chalcogenide anions forming a trigonal prism about the cation and the additional anion capping one of the rectangular faces. Figure 2 is a view of the lattice

0022-4596/93 $5.00

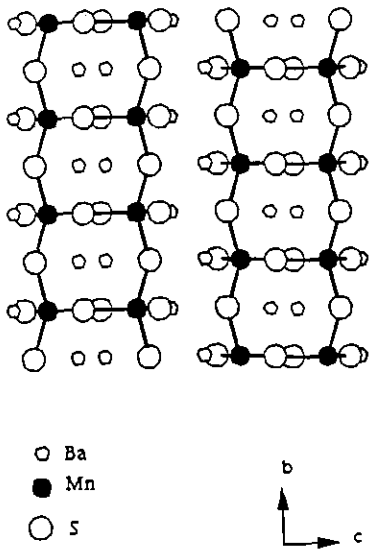

FIG. 1. Illustration of the structure of Ba_2MnS_3 viewed perpendicular to the chain axis.

of Ba_2MnS_3 looking down the b axis (at a slight angle) to illustrate the separation of the linear chains by the barium cations. The shortest Mn–Mn distance between adjacent chains is 5.96, 6.61, and 6.31 Å in the sulfide, selenide, and telluride respectively (*1*, *3*). Due to the symmetry of the space group, *Pnma*, the distances between Mn atoms along the a and c axis are equal to the unit cell length in these directions. There are no significant X–X contacts in these phases. Each chalcogenide atom is surrounded by a distorted octahedron of Ba and Mn atoms with no chalcogenide nearest neighbors.

We felt that the Ba_2MnX_3 phases are ideal for studying linear-chain antiferromagnetism, if one could make solid solutions of the single-chalcogenide phases, i.e., $Ba_2MnS_{3-x}Se_x$, and $Ba_2MnSe_{3-x}Te_x$ ($0 \leq x \leq 3$). This would allow one to study the interplay between two opposing influences upon the strength of the Mn–Mn magnetic coupling: the geometric effect of the incorporation of larger bridging atoms and the electronic influence of the bridging-atom electronegativity/polarizability. Generally speaking, the magnetic exchange between paramagnetic centers is stronger through more polarizable, less electronegative bridging atoms (*4*). This trend has been observed in the binary manganese chalcogenides MnX (X = S, Se, Te) in which the magnetic ordering transitions occur at 122, 125 and 173 K respectively (*5*). Based upon this influence, one would expect the magnetic exchange to be greater through bridging selenide rather than through sulfide. Grey and Steinfink found that the opposite was observed in the case of Ba_2MnS_3 versus Ba_2MnSe_3 (*1*). The observed coupling constants of the sulfide ($J = -12$ K) was larger than that of the selenide ($J = -10$ K). Since the Mn–Mn distance in Ba_2MnS_3 is 4.31 Å and 4.47 Å in Ba_2MnSe_3, the difference in the coupling constants is attributed to the strong dependence of the magnetic superexchange upon the Mn–Mn distance (*6*). In this latter case the geometric factor is domi-

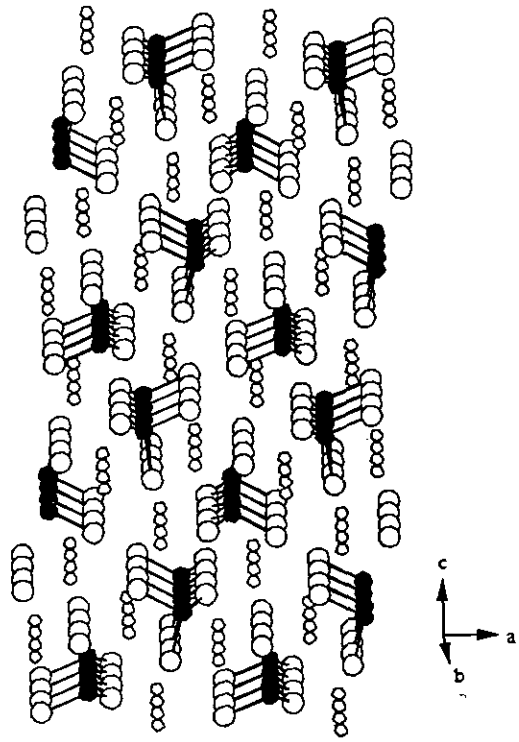

FIG. 2. Illustration of the structure of Ba_2MnS_3 viewed down the chain axis.

nant. We were curious, first whether or not the telluride phase Ba_2MnTe_3 would behave as a linear chain antiferromagnet; and if so, would the presence of the highly polarizable, nearly metallic telluride bridge overcome the geometric influence of its larger radius? In addition, the study of linear-chain materials containing chalcogenide anions as the superexchange pathway (especially Se, Te) has received little attention relative to the number of structures containing halides and oxides. For these reasons, we undertook the synthesis and characterization of the $Ba_2MnX_xX'_{3-x}$ (X = S, Se, Te) phases and studied their electrical transport and magnetic properties.

Experimental

The solid solutions $Ba_2MnS_xSe_{3-x}$ and $Ba_2MnSe_xTe_{3-x}$ were prepared by reacting stoichiometric quantities of manganese (Aesar, 99.999%), sulfur (Aldrich, 99.999%), selenium (Aesar, 99.9%), tellurium (Aldrich, 99.99%), barium sulfide (Cerac, 99.99%), barium selenide (Cerac, 99.99%) and barium telluride (Cerac, 99.99%). The following stoichiometries were used. For sulfur-rich phases, $Ba_2MnS_xSe_{3-x}$ ($x > 2.0$):

$$2\,BaS + Mn + (x - 2)\,S + (3 - x)\,Se;$$

for selenium-rich phases:

$$2\,BaSe + Mn + (x - 2)\,Se + (3 - x)\,S \rightarrow Ba_2MnSe_xS_{3-x}\ (x > 2.0),$$

$$2\,BaSe + Mn + (x - 2)\,Se + (3 - x)\,Te \rightarrow Ba_2MnSe_xTe_{3-x}\ (x > 2.0);$$

and for tellurium-rich phases:

$$2\,BaTe + Mn + (x - 2)\,Te + (3 - x)\,Se \rightarrow Ba_2MnTe_xSe_{3-x}\ (x > 2.0).$$

Approximately one gram of thoroughly mixed starting material was loaded into a cylindrical graphite crucible (10 cm × 2.5 cm o.d. × 1.5 cm i.d.) inside of a quartz glass tube. The graphite inner tube was necessary to prevent attack of the BaX starting materials upon the outer quartz glass tube. The tubes were then degassed several times employing evacuation/Argon refill/evacuation cycles and sealed under vacuum (10^{-4} Torr). The tubes were slowly (20°C/hr) heated in a tube furnace to 450°C, held at this temperature for 48 hr, then heated to 800–1050°C and held at this temperature for 72 hr. Due to the melting points of the products (900–1100°C), and the tendency towards incongruent melting, the sulfide rich phases required the highest reaction temperatures (1000–1050°C) whereas the tellurides required the lowest temperatures (800–850°C) to achieve homogeneous products. The orange-brown (sulfide) to black (telluride) products were then reground, pressed into pellets (7000 psi) and annealed for 96 hr at 800–900°C under vacuum in quartz glass tubes with a protective graphite coating. A thin graphite film was produced in each tube by pyrolizing acetone (in air) in each tube with a propane flame.

The microcrystalline products were characterized by determination of their X-ray powder diffraction profiles, which were obtained on a Scintag PAD V diffractometer using Ni-filtered Cu$K\alpha$ radiation. Silicon was used as an internal standard to provide corrected d-spacings and the unit cell parameters were refined by least-squares methods. Room temperature resistivity measurements were performed on sintered pellets with a conventional four-probe technique. Electrical contacts were made with gold wire and silver epoxy. Magnetic measurements were conducted in a SQUID, Quantum Design magnetometer. Thin pieces cut from sintered pellets were oriented with the magnetic field of 1000 gauss parallel to the plate axis to minimize demagnetization effects.

Results and Discussion

The products obtained as described above were dark orange-brown to black microcrystalline solids which are stable indefi-

TABLE I

CELL CONSTANTS OF THE MIXED CHALCOGENIDE PHASES: $Ba_2MnX_xX'_{3-x}$ (X, X' = S, Se, Te; x = 0, 1, 2)

Phase	a (Å)	b (Å)	c (Å)
Ba_2MnS_3	8.818(5)	4.306(4)	17.040(9)
$Ba_2MnS_2Se_1$	8.911(6)	4.367(3)	17.279(8)
$Ba_2MnS_1Se_2$	9.018(4)	4.406(3)	17.507(10)
Ba_2MnSe_3	9.138(4)	4.469(3)	17.730(9)
$Ba_2MnSe_2Te_1$	9.332(5)	4.547(5)	18.143(8)
$Ba_2MnSe_1Te_2$	9.518(6)	4.651(4)	18.509(7)
Ba_2MnTe_3	9.693(5)	4.729(5)	18.891(9)

nitely in dry air but decompose slowly upon exposure to moist air. The powder X-ray diffraction data were indexed based upon an orthorhombic cell with the space group *Pnma*. The lattice parameters as a function of the chalcogenide content of the mixed-chalcogenide solid solutions are tabulated in Table I. The cell constants of the single-chalcogenide containing members agree well with previously reported values (*1*, *3*), with the intermediate compositions exhibiting cell constants consistent with the formation of solid solutions throughout the full range of composition.

Room temperature resistivity measurements demonstrate that all of these phases are insulators with room temperature resistivities of 10^2–10^3 Ω cm. No attempt to obtain temperature dependent resistivity data was made due to the high room temperature resistivities.

The magnetic susceptibility and inverse susceptibility as a function of temperature of the Ba_2MnTe_3 is plotted in Fig. 3 and is typical of all of the mixed-chalcogenide solid solutions. No corrections for diamagnetic contributions or temperature independent paramagnetism were made to the susceptibility data. Magnetic constants derived from these data are tabulated in Table II. The Weiss constants (θ) and the effective magnetic moments were determined by a Curie–Weiss fit of the linear, high temperature portion (200–300 K) of the inverse susceptibility curve. The values for the temperature of the maximum of the susceptibility (T_{max}) were determined by taking the first derivative of the susceptibility versus temperature curve.

Several trends are clear in the derived magnetic constants for the solid solutions $Ba_2MnX_{3-x}X'_x$ (X, X' = S, Se, Te). All of these phases exhibit broad maxima in the χ vs T plots indicative of one-dimensional magnetic ordering. The Weiss constants of these phases are all less than zero suggesting antiferromagnetic coupling between the Mn^{2+} ions. The absolute values of the Weiss constants are indicative of the strength of this antiferromagnetic coupling, dropping significantly through the series as sulfur (θ = −317 K) is replaced by selenium (θ(−217 K) = −217 K) and then by tellurium (θ(−142 K) = −142 K).

A second parallel trend in the magnetic data is the variation of the temperature at which the maximum in the magnetic susceptibility (T_{max}) occurs. The stronger the antiferromagnetic coupling along the chains (as reflected by $|\theta|$), the higher the temperature at which the bulk magnetic susceptibility begins to diminish. This maximum in the magnetic susceptibility and the subsequent decline in susceptibility is due to the gradual build-up of short-range magnetic ordering, which at some characteristic temperature (T_{max}) overcomes the normal inverse correlation between the temperature and the magnetic susceptibility as defined by the Curie law.

As previously discussed in the introduction, it is possible to model the magnetic susceptibility behavior of linear-chain antiferromagnets. Assuming that the phases Ba_2MnX_3 can be treated as one-dimensional Heisenberg antiferromagnets in which the Mn^{2+} ions have a spin, $S = \frac{5}{2}$, it should be possible to use Eq. (1) to fit the observed magnetic susceptibility data and thereby determine the coupling constant (J) and the g-value of each of these phases. The derived equation for the magnetic susceptibility (χ) as a function of temperature (T) is:

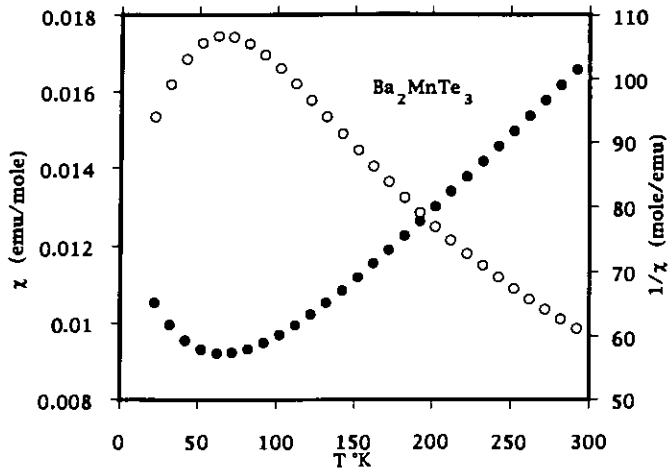

FIG. 3. Temperature dependence of the magnetic susceptibility (○) and inverse susceptibility (●) of Ba_2MnTe_3.

$$\chi = \frac{Ng^2\mu_B^2 S(S+1)}{3kT} \cdot \frac{1-U}{1+U}, \qquad (1)$$

where $U = (T/T_0) - \coth(T_0/T)$, $T_0 = 2JS(S+1)/k$, N = Avogadro's number, g = Landé constant, μ_B = Bohr magneton, S = spin ($Mn^{2+} = \frac{5}{2}$), and k = Boltzmann constant (*2*). As is customary, J, the coupling constant, is defined as negative for antiferromagnetic coupling. The magnetic susceptibility data was fit for each of the solid solutions by varying both the J- and g-values in Eq. 1 to determine the values which produced the best agreement between the calculated and observed magnetic susceptibility above T_{max}. The fit below T_{max} is not expected to be as good, due to the emergence of three-dimensional magnetic ordering effects as the temperature is lowered (*4*). The calculated and observed magnetic susceptibility curves of the Ba_2MnTe_3 are shown in Fig. 4. This is representative of the agreement between the calculated and observed magnetic susceptibility of the mixed-chalcogenide solid solutions as well.

TABLE II

MAGNETIC PARAMETERS OF THE MIXED-CHALCOGENIDE PHASES: $Ba_2MnX_xX'_{3-x}$ (X, X' = S, Se, Te)

Composition	T_{max} (K)	θ^a (K)	$\mu_{eff}{}^a$ (μ_B)	$\chi_{rt}{}^b$ ($\times 10^{-3}$ emu/M)	J/k^c (°K)	g^c	Mn–Mn (Å)
S_3	100	−317	4.62	8.7	−12.3	2.00	4.31
S_2Se	91	−278	4.72	8.9	−11.5	2.00	4.37
SSe_2	85	−253	4.75	9.0	−10.7	2.01	4.41
Se_3	80	−217	4.86	9.5	−9.8	2.01	4.47
Se_2Te	74	−192	4.84	9.3	−9.1	2.01	4.55
$SeTe_2$	68	−176	4.84	9.3	−8.3	2.00	4.65
Te_3	62	−142	4.82	9.6	−7.6	2.01	4.73

[a] Determined from Curie–Weiss fit of $1/\chi$ vs T plot.
[b] χ_{rt} is the room temperature magnetic susceptibility.
[c] Determined from curve-fitting of χ vs T using Bonner–Fisher Model.

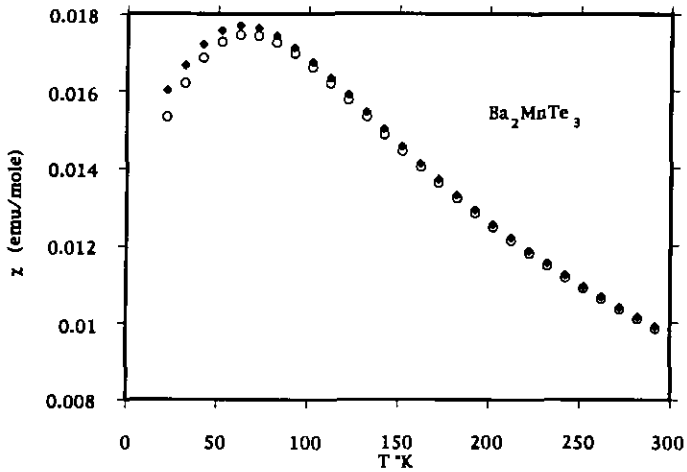

FIG. 4. Observed (○) and calculated (◆) magnetic susceptibility of Ba_2MnTe_3 versus temperature. Calculation based upon the Bonner and Fisher Model (*2*).

The best values for J and g are tabulated in Table II along with the previously derived magnetic constants (θ, μ_{eff}, T_{max}) as well as the intrachain metal–metal distance (b lattice dimension).

Overall, the agreement between the observed and calculated magnetic susceptibility data is excellent above T_{max} (Fig. 4). This confirms the adequacy of assuming that the magnetic ordering in these phases is predominantly one-dimensional and that the Mn^{2+} ions are behaving as isotropic Heisenberg paramagnets. A significant decrease in the absolute value of the coupling constant, J, as the larger chalcogenides are incorporated into the lattice is observed.

Since the mechanism of the magnetic coupling along the chains is likely via superexchange through the diamagnetic chalcogenide atoms, the trends in the temperature of the maximum susceptibility, the Weiss constants and the coupling constants are explicable in terms of the progressively longer superexchange pathways in the solid solutions from Ba_2MnS_3 to Ba_2MnTe_3. The intrachain Mn–Mn distance (which is directly related to the superexchange path) is equal to the b dimension of the unit cell. Table II clearly shows the increase of the b dimension as the larger chalcogenides are incorporated into the lattice. Magnetic coupling via the superexchange mechanism is strongly dependent upon the distance between interacting ions, in some cases, $J = 1/r^{(12)}$, where r is the distance between paramagnetic ions (*4*). This strong distance dependence is evident here, a fit of the coupling constants to a power law dependence indicates that $J = 1/r^5$. A 38% drop in the magnetic coupling constant between Ba_2MnTe_3 (−7.6 K) and Ba_2MnS_3 (−12.3 K) is paralleled by only a 10% change in the Mn–Mn distance (4.31 vs 4.73 Å).

In addition to a monotonic increase in the superexchange pathway length, as the larger chalcogenides are incorporated into the Ba_2MnX_3 phases, there is also a reduction of the Mn–X–Mn bridging angle: S = 119.8°, Se = 118.5° and Te = 116.3° (*1*, *3*). If the magnetic coupling by bridging chalcogenides is through p orbitals, one would predict antiferromagnetic coupling based upon the Goodenough (*7*) and Kanamori rules (*8*). This coupling would be strongest with a bridging angle of 90°. If however, s orbitals are the superexchange pathway, then one would expect ferromagnetic coupling. Consequently, an increase in the bridging angle from 90° results in a decrease in the strength of the antiferromagnetic coupling due to the

increase in the s-character of the bridging orbitals. Numerous examples consistent with this correlation of magnetic coupling and bridging angles have been published (*9*). In the present case, the opposite trend is observed: as the bridging angle is reduced in the series sulfur through tellurium, the magnetic coupling also diminishes. This may be the consequence of mixing-in of low-lying *d*-orbitals of the chalcogenides which would invalidate the simplistic orbital arguments above, or may suggest other hybridizations for the bridging chalcogenide atoms (*10*). The observation that the strongest magnetic coupling occurs through a nearly 120° Mn–S–Mn bridge suggest a sp^2 hybridization for the chalcogenide. Any deviation from the ideal 120° angle would lead to lower orbital overlap and a weakened magnetic coupling through these bonds.

The effect of the variation in the chalcogenide content upon the effective magnetic moment (μ_{eff}) is consistent with the diminished orbital overlap argument for the larger chalcogenides. First, it should be noted that the calculated μ_{eff} at 300 K ($\mu_{eff} = (8\chi T)^{1/2}$) for Ba_2MnS_3 (4.57 μ_B) and Ba_2MnSe_3 (4.77 μ_B) in the present study both agree closely with the values previously reported by Steinfink *et al.* 4.64 μ_B and 4.90 μ_B respectively (*1*). These calculated μ_{eff} values are low for a $s = \frac{5}{2}$ Mn^{2+} ion which typically exhibits spin-only effective magnetic moments of 5.5–6.0 μ_B; suggesting that a significant amount of linear chain antiferromagnetic coupling is occurring even at 300 K, or else a significant amount of ligand to metal charge transfer (LMCT) is occurring to effectively diminish the magnetic moment of the Mn^{2+} ion. The covalency of Mn chalcogenide bonds generally increases in the series sulfur through tellurium, resulting in greater LMCT and smaller magnetic moments for Mn^{2+} (*11*). In the present case, the opposite trend is observed and may be the consequence of diminished orbital overlap. The poorer orbital overlap of the heavier chalcogenides due to geometric constraints results in less LMCT and therefore larger effective magnetic moments.

One final observation regarding these sets of curves is that below T_{max}, the observed magnetic susceptibility of the phases is consistently lower than the calculated value, with greater deviations as the temperature is lowered. This suggests that at lower temperatures, three-dimensional ordering is occurring. This same behavior is observed in TMMC, which eventually undergoes an antiferromagnetic phase transition at 6.7 K (*12*, *13*). The observed decrease in magnetic susceptibility implies that the spins on adjacent chains begin to become correlated, probably through dipole–dipole interactions. Figure 5 illustrates an expanded view of the low temperature susceptibility of the phases: Ba_2MnX_3 (X = S, Se, Te) from 22–2 K. Note that all three of these phases exhibit an upturn in susceptibility at very low temperatures ($T < 5$ K), but do not show any new maxima, typical of an antiferromagnetic ordering of the type observed in TMMC. It is possible that the absence of a new maximum in the low temperature region indicates that these phases are ordering ferromagnetically rather than antiferromagnetically as in TMMC, though it may also be that the Neél temperature is below 2 K. The lowest temperature points in the Ba_2MnS_3 curve hint at a maximum of 2.5 K. Of the three phases, Ba_2MnS_3 would be expected to show the highest temperature three-dimensional ordering brought about by dipolar interactions since it has the shortest interchain separation. This suggests that the ratio of intrachain to interchain magnetic interactions is on the order of 10^4 (*14*). Alternatively, the low temperature susceptibility behavior may be a consequence of structural defects or the ubiquitous "Curie tails" commonly observed at low temperature.

Conclusion

The linear chain antiferromagnetism previously reported by Steinfink[1] for Ba_2MnS_3

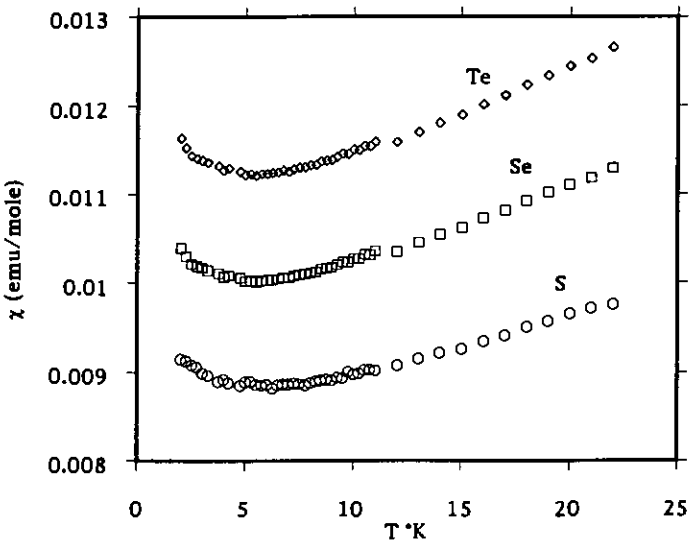

FIG. 5. Plot of the low temperature magnetic susceptibility of the Ba_2MnX_3 (X = S, Se, Te) phases.

and Ba_2MnSe_3 has now been demonstrated for Ba_2MnTe_3. The mixed-chalcogenide solid solutions $Ba_2MnX_xX'_{3-x}$ (X, X' = S, Se, Te; x = 0, 1, 2) have been prepared and their electrical and magnetic properties studied. All of the phases are insulating with room temperature resistivities of approximately 10^2–10^3 Ω cm. The magnetic susceptibility curves of these mixed-chalcogenide phases exhibit broad maxima typical of one dimensional magnetic ordering. The linear-chain model of Bonner–Fisher (*2*) for Heisenberg-type ions was applied to the susceptibility data. It was observed that the magnitude of the magnetic coupling constant, J, was inversely proportional to the Mn–Mn distance along the chains. This is consistent with the assumption that the magnetic interactions in these chains occur through a superexchange mechanism. If one assumes a sp^3 hybridization of the bridging chalcogenides, the trend in the exchange coupling can also be rationalized in terms of the degree of deviation of the bridging Mn–X–Mn angle from the ideal of 120°. Either, or both, of the geometric influences are dominant over the influence of the bridging atom polarizability in determining the strength of the magnetic coupling in these phases. At temperatures below T_{max}, the magnetic susceptibility deviates from the Bonner–Fisher model, and this is attributed to dipolar interactions, as observed in TMMC (*13*). No clear three-dimensional phase transition above 3 K is observed, though in Ba_2MnS_3, a maximum at 2.5 K is suggested.

References

1. I. E. GREY AND H. STEINFINK, *Inorg. Chem.* **10,** 691 (1971).
2. J. C. BONNER AND M. E. FISHER, *Phys. Rev. A* **135,** 640 (1964).
3. P. MATJE, W. MÜLLER, AND H. SCHÄFER, *Z. Naturforsch. B* **32,** 835 (1977).
4. R. L. CARLIN, "Magnetochemistry," Chap. 7, pp. 163–225. Springer-Verlag, Berlin, 1986.
5. R. RITTER AND L. JANSON, *Phys. Rev. B* **8,** 2139 (1973).
6. L. J. DEJONGH AND R. BLOCK, *Physica B* **79,** 568 (1975).
7. J. B. GOODENOUGH, "Magnetism and the Chemical Bond," Interscience, New York, 1963.
8. J. KANAMORI, *J. Phys. Chem. Solids* **10,** 87 (1959).
9. D. J. HODGSON, *in* "Progress in Inorganic Chemistry" (S. J. Lippard, Ed.), Vol. 19. Interscience, New York, 1976.

10. Y. Journaux, O. Kahn, J. Zarembowitch, J. Galy and J. Jaud, *J. Am. Chem. Soc.* **105,** 7585 (1983).

11. R. D. Shannon and H. Vincent, "Structure and Bonding," Vol. 19. Springer-Verlag, New York, N.Y., 1974.

12. L. J. de Jongh, A. R. Miedema, *Adv. Phys.* **23,** 1 (1974).

13. R. Dingle, M. E. Lines, S. L. Holt, *Phys. Rev.* **187,** 643 (1969).

14. T. Oguchi, *Phys. Rev. A* **133,** 1098 (1964).